

Spin-Valley Polarized Quantum Anomalous Hall Effect and a Valley-Controlled Half Metal in Bilayer Graphene

Xuechao Zhai^{1,2}, Yaroslav M. Blanter²

¹New Energy Technology Engineering Laboratory of Jiangsu Province & School of Science, Nanjing University of Posts and Telecommunications (NJUPT), Nanjing 210023, China

²Kavli Institute of NanoScience, Delft University of Technology, 2628 CJ Delft, The Netherlands
(Dated: November 15, 2019)

We investigate topological phases of bilayer graphene subject to antiferromagnetic exchange field, interlayer bias, and irradiated by light. We discover that at finite bias and light intensity the system transitions into a previously unknown spin-valley polarized quantum anomalous Hall (SVP-QAH) insulator state, for which the subsystem of one spin is a valley Hall topological insulator (TI) and that of the other spin is a QAH insulator. We assess the TI phases occurring in the system by analytically calculating the spin-valley dependent Chern number, and characterize them by considering edge states in a nanoribbon. We demonstrate that the SVP-QAH edge states lead to a unique spin rectification effect in a domain wall. Along the phase boundary, we observe a bulk half-metal state with Berry's phase of 2π .

Introduction. Bernal-stacked bilayer graphene (BLG) consists of two honeycomb lattices coupled by van der Waals interaction [1]. Due to its novel electronic properties, such as low-energy states with Berry's phase of [2] 2π and an electrically-tunable band gap [3, 4], BLG has recently attracted much attention both theoretically and experimentally, see *e.g.* Refs. 5–10. In particular, BLG became popular for studies of phenomena related to the valley degree of freedom [9, 11–14], resulting in discovery of non-trivial topological states of matter. Recently, a striking finding was the discovery of the quantum valley Hall (QVH) effect in BLG, for which the edge states in the gap driven by an interlayer bias are valley-polarized and provide the conductance quantization with the step of [15–18] $4e^2/h$. Theoretical studies have predicted that the usual QVH insulator in BLG undergoes a transition to a valley-polarized quantum spin Hall insulator under effect of Rashba spin-orbit interaction [19, 20].

Another attractive topological state of matter is the quantum anomalous Hall (QAH) state, generally characterized by chiral edge states in the gap and nonzero charge Chern numbers [21–23]. The QAH state in BLG has been suggested to be induced by Rashba interaction and internal magnetization [24] or by strong circularly polarized light [25–27], differently from the mechanism of Landau-level quantization in quantum Hall effect. Most recently, the valley-polarized QAH state possessing the properties of both the QVH and QAH states has been proposed in other 2D systems [28, 29] similar to BLG. Interestingly, this QAH state can possess edge states which are not completely chiral [28].

In this Letter, we present the light and voltage controlled phase diagram of BLG in contact with layered antiferromagnetic (AFM) exchange field and discover a variety of topological insulator (TI) states in this system. We argue that this AFM BLG itself is a quantum anomalous valley Hall (QAVH) insulator [30], that it undergoes a transition to a usual QVH insulator as interlayer bias increases, and that it is switched to a normal QAH (N-QAH) insulator, a system with chiral edge states, as light intensity increases. Remarkably, we discover that if both voltage and light are applied, the system can be in

a spin-valley polarized QAH (SVP-QAH) insulator state, for which the subsystem of one spin is in a QVH state and that of the other spin is in a QAH state. To our knowledge, this state has not been previously described in the literature and it is distinct from the single-valley spin-polarized QAH states [26, 29] and the QAH states with no spin or valley polarizations [13–17, 21–23, 28].

The TI states in the system are discriminated by the spin-valley dependent Chern number [9], which we calculate analytically. We further characterize these TIs by edge states in a zigzag ribbon and show transport differences in domain walls. In the phase boundary, we discover that the 2D bulk system can host a half-metal state with Berry's phase of 2π , and the number of gap-closing valleys is tunable.

Hamiltonian. The BLG system we consider is described by the eight-band tight-binding model

$$\begin{aligned} \hat{H} = & -J \sum_{\langle i,j \rangle_{\parallel} \alpha} c_{i\alpha}^{\dagger} c_{j\alpha} - \gamma \sum_{\langle i,j \rangle_{\perp} \alpha} c_{i\alpha}^{\dagger} c_{j\alpha} + M \sum_{i\alpha} \mu_i c_{i\alpha}^{\dagger} \sigma_z c_{i\alpha} \\ & - U \sum_{i\alpha} \mu_i c_{i\alpha}^{\dagger} c_{i\alpha} + i \frac{\lambda}{3\sqrt{3}} \sum_{\langle\langle i,j \rangle\rangle_{\parallel} \alpha} v_{ij} c_{i\alpha}^{\dagger} c_{j\alpha}, \end{aligned} \quad (1)$$

where $c_{i\alpha}^{\dagger}$ creates an electron with spin polarization α at site i , and $\langle i, j \rangle / \langle\langle i, j \rangle\rangle$ run over all the nearest and next nearest neighbor hopping sites. The subscript \parallel (\perp) denotes “in plane” (“out of plane”), $\mu_i = \pm 1$ indicates that site i lies in the bottom (top) layer, σ_z is the z -component of Pauli matrix in the spin subspace, and $v_{ij} = +1$ (-1) holds if the next nearest hopping is anticlockwise (clockwise). In Eq. (1), the first and second terms are the intralayer and interlayer nearest neighbor hoppings with [8] $J = 3.0$ eV and $\gamma = 0.39$ eV. The third term, H_M , is the layered AFM exchange field, which can be applied by depositing BLG between 2D magnetic insulators CrI_3 [30] ($M \sim 7$ meV can be achieved). The fourth term, H_U , is the interlayer bias with U being up to 125 meV in experiment [4, 7]. The fifth term, H_{λ} , is the Haldane mass term [31], which can be applied [26] by irradiating BLG with circularly polarized light (see Supplemental Material [32] and Refs. [33, 34]). Estimated from the band width in BLG, the

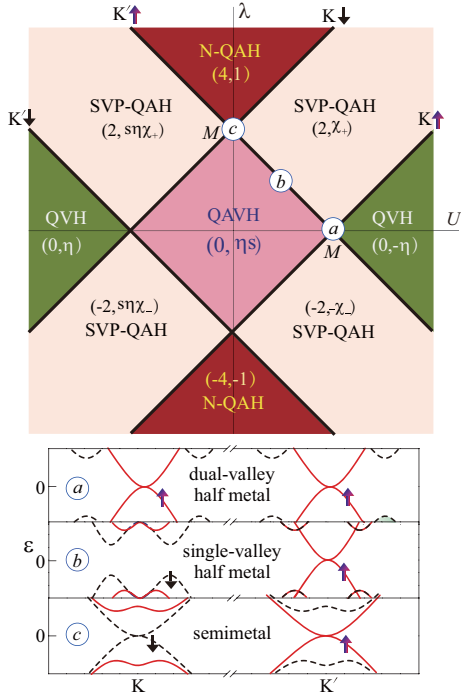


FIG. 1: (Color online) Phase diagram in the U - λ plane (top). The Chern numbers (C, C_η^s) are used to index the TI phases. For the SVP-QAH state, $C_\eta^s = \chi_\pm = (\delta_{s,1} + \delta_{s,-1})(\delta_{s,1} \pm s\eta\delta_{s,-1})$ [see Eq. (11)]. Bold lines represent the phase boundaries, where gap closing is indexed by K (K') and \uparrow (\downarrow). The bulk bands for points a - c are shown at the bottom, where solid (dashed) lines denote \uparrow (\downarrow) subbands.

light frequency would typically lie in the range [26, 32] 10^{13} – 10^{14} Hz, leading to the estimate of $\lambda \sim 10$ meV.

Topological theory. The QAH effect is characterized by the charge Chern number [21–24, 28]

$$C = \frac{1}{2\pi} \sum_n \int_{\text{BZ}} d^2k \Omega_n(\mathbf{k}), \quad (2)$$

where Ω_n is the momentum-space Berry curvature [9] in the out-of-plane direction for the n -th subband

$$\Omega_n(\mathbf{k}) = - \sum_{n' \neq n} \frac{2\text{Im} \langle \psi_{nk} | v_x | \psi_{n'k} \rangle \langle \psi_{n'k} | v_y | \psi_{nk} \rangle}{(\epsilon_{n'} - \epsilon_n)^2}. \quad (3)$$

The summation is over all occupied valence bands in the first Brillouin zone below the bulk band gap, ψ is the Bloch state, and $v_{x(y)}$ is the velocity operator along the x (y) direction.

One can label a state a TI if it has at least one nonzero topological invariant [24–27, 29–31, 33, 34]. Because electrons in BLG here have a mixture of charge, spin and valley degrees of freedom, the index C can not identify the spin or valley polarized TI phases. To solve this problem, we employ a decomposed, spin and valley dependent Chern number [9, 34] C_η^s , which is well defined in half of the first Brillouin zone around K ($\eta = +1$) or K' ($\eta = -1$) points for spin-up ($s = +1$) or spin-down ($s = -1$) electrons. On basis of C_η^s , the spin and valley Chern numbers [9] can be defined as $C_S = C_\uparrow - C_\downarrow =$

$\sum_\eta (C_\eta^\uparrow - C_\eta^\downarrow)$ and $C_v = C_K - C_{K'} = \sum_s (C_K^s - C_{K'}^s)$, respectively. The charge Chern number satisfies $C = \sum_{\eta,s} C_\eta^s$.

Phase diagram. We present our result as the phase diagram in Fig. 1 by tuning U and λ . The topological numbers (C, C_η^s) are used to index the TI phases, including QAVH, QVH, N-QAH and SVP-QAH. We show how to derive the analytical expressions for the phase boundary and the Chern numbers from low-energy theory later. Because the sign changes of U and λ only influence the signs of Chern numbers (no novel phases appear), one only needs to characterize the phases for ($U \geq 0, \lambda \geq 0$). To describe the edge states, some typical cases are chosen to calculate the bands in a zigzag ribbon (Supplemental Material [32]). The edge states in real space for each TI are illustrated in Figs. 2(a)-2(d), where the moving directions (hollow arrows) for electrons agree with Eqs. (9-12). At the phase boundary, the bulk gap closes [Eq. (6)].

We first discuss the QAVH state, for which $(C, C_\eta^s) = (0, \eta s)$ [30]. The nonzero value of C_η^s in this phase arises from the inversion symmetry breaking dominated by M . Although the QAVH phase has metallic in-gap edge states near K and K' , the index C is zero. The anomalous property of the state is that the subsystem of each spin is a QVH insulator [$C_v^\uparrow = C_K^\uparrow - C_{K'}^\uparrow = C_{K'}^\downarrow - C_K^\downarrow = -C_v^\downarrow = 2$ in Fig. 2(a)], while the whole system is not valley polarized ($C_v = 0$). The result $C_K^\uparrow + C_{K'}^\downarrow = C_{K'}^\uparrow + C_K^\downarrow = 0$ indicates the edge states in each valley behaves as a quantum spin Hall state [19, 22] in spite of $C_S = 0$. If we include non-zero voltage U , the system eventually undergoes a transition to a normal QVH insulator [$C_v = -4$ in Fig. 2(b)] due to the competition of U and M . The QAVH insulator transitions to an N-QAH insulator [$C = 4$ in Fig. 2(c)] as λ increases due to the time-reversal symmetry breaking. Each transition is associated with with a process of the closing and reopening of the gap.

Our most significant result is the SVP-QAH phase, which appears in regions where $U\lambda \neq 0$ and occupies a major part of the phase diagram. For a SVP-QAH state, four spin-down edge states in the gap appear near K and K' , but four spin-up edge states appear away from K and K' [Figs. 2(d) and 2(g)]. Correspondingly, the Berry curvature in the (k_x, k_y) plane [Fig. 2(e)] and specifically along K - K' direction [Fig. 2(f)] is shown. We find that the spin-down subsystem is a QVH insulator [$C_K^\downarrow = -C_{K'}^\downarrow = -1, C_v^\downarrow = -2, C^\downarrow = C_K^\downarrow + C_{K'}^\downarrow = 0$], whereas the spin-up subsystem is a normal QAH insulator [$C_K^\uparrow = C_{K'}^\uparrow = 1, C_v^\uparrow = 0, C^\uparrow = C_K^\uparrow + C_{K'}^\uparrow = 2$], and then $C = -C_v = C_S = 2$ is achieved. To our knowledge, this SVP-QAH insulator is a new type of a QAH state, which differs obviously from the single-valley spin-polarized QAH [26, 29], spin-unpolarized QAH [9, 12–14, 28], and valley-unpolarized QAH [9, 22, 34] states discovered previously.

At the phase boundaries, see bold lines in Fig. 1, there exists a 2D bulk state that is half-metallic [35] (gap closing at K or K'), as shown by the completely spin-polarized band structures (bottom) near the Fermi level for the marked points a and b . In contrast, point a corresponds to a dual-valley half-metal (valley degeneracy), while point b refers to a single-valley

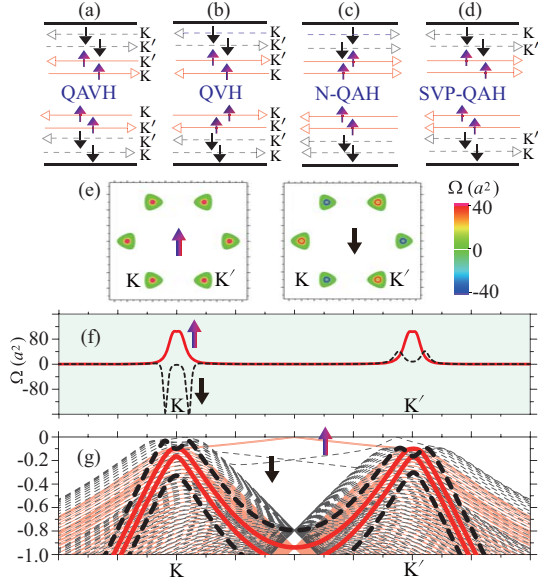


FIG. 2: (Color online) (a)-(d) Schematics of eight edge states in the bulk gap for four TIs in Fig. 1, corresponding to our calculated band structures [32] of a zigzag-edged ribbon for typical points under ($U \geq 0, \lambda \leq 0$). (e)-(g) Electronic properties of the SVP-QAH state. Berry curvature in (e) (k_x, k_y) plane and (f) along K - K' direction, corresponding to (g) the bulk (thick lines) and ribbon (thin lines) bands.

half-metal (the other valley is insulating). For the marked point c , spin-down (spin-up) subbands near the Fermi level are locked to the K (K') valley, resulting in a spin-valley locked semimetal. Thus gap closing of the valleys in which one or two is tunable. Notably, the bulk half-metal state here has the Berry's phase of 2π [Eq. (8)].

Low-energy formalism. To further explore the physics underlying the phase diagram, we analyze the low-energy effective Hamiltonian derived from the lattice model (1) after Fourier transformation, and reveal the physics of electrons near K and K' . For simplicity, we set $\hbar = 1$ and $v_F = 1$ below. Because two opposite spins are decoupled in Eq. (1), the effective Hamiltonian can be written as a 4×4 matrix

$$\mathcal{H}_k = \begin{pmatrix} \Delta_{\eta s}^+ - U, & \eta k_x - ik_y, & 0, & 0 \\ \eta k_x + ik_y, & -\Delta_{\eta s}^- - U, & -\gamma, & 0 \\ 0, & -\gamma, & \Delta_{\eta s}^- + U, & \eta k_x - ik_y \\ 0, & 0, & \eta k_x + ik_y, & -\Delta_{\eta s}^+ + U \end{pmatrix}, \quad (4)$$

where $\Delta_{\eta s}^\pm = \eta\lambda \pm sM$. Note that s and M only occur as a product sM , and thus the reversal of the sign of M is equivalent to the reversal of spin orientation. We will assume $M > 0$. By matrix diagonalization, we derive the band structure as

$$\varepsilon = \pm \sqrt{k^2 + (sM - U)^2 + \lambda^2 + \frac{1}{2}(\gamma^2 \pm \sqrt{\Gamma_k})}, \quad (5)$$

$$\Gamma_k = k^2[16(sM - U)^2 + 4\gamma^2] + [\gamma^2 - 4\eta\lambda(sM - U)]^2.$$

Note that the electron-hole symmetry is present in Eq. (5), from which one can prove that the gap is closed only under

$\varepsilon = 0$, which requires $k = 0$ [at $K(K')$] and simultaneously

$$U = sM + \eta\lambda. \quad (6)$$

According to the topological theory [9], this gap-closing condition in Eq. (6) precisely describes the phase boundary as given in Fig. 1. Specifically at $k = 0$, the energy gap reads

$$\Delta_\eta^s = 2\sqrt{(sM - U)^2 + \lambda^2 + \frac{1}{2}(\gamma^2 - |\gamma^2 - 4\eta\lambda(sM - U))}. \quad (7)$$

Judging from Eq. (6), the system is a dual-valley half-metal for $(\lambda, U) = (0, \pm M)$ and a spin-valley locked semimetal for $(\lambda, U) = (\pm M, 0)$. Except for these points, the system is a single-valley half-metal in the phase boundary. For the half-metal state, Hamiltonian (4) for specific spin recovers the usual case of BLG without external fields. The effective 2×2 Hamiltonian used in Ref. 2 can be derived to describe the low-energy half-metal subbands with parabolic dispersion. The half-metal Bloch state $\psi_{k,\phi}$ (ϕ being the azimuthal angle of the momentum) here has the Berry phase [36]

$$\varphi_B = i \int_0^{2\pi} d\phi \langle \psi_{k,\phi} | \frac{\partial}{\partial \phi} | \psi_{k,\phi} \rangle = 2\eta\pi, \quad (8)$$

which can induce a spin-polarized integer quantum Hall effect with a missing zero-level plateau [2].

Chern numbers and domain-wall transport. We see from Eq. (6), Fig. 1 and our band calculations [32] that the QAVH, QVH, N-QAH and SVP-QAH insulator states hold under $|\lambda| < M - |U|$, $|\lambda| < |U| - M$, $|\lambda| > |U| + M$, $||U| - M| < |\lambda| < |U| + M$, respectively. Usually, the topological invariants are associated with the signs of the parameters for a TI state [9, 34]. For the QAVH, QVH, and N-QAH insulators here, the index C_η^s is respectively determined by

$$C_\eta^s = \eta s, \quad -\eta \text{sgn}(U), \quad \text{sgn}(\lambda) \quad (9)$$

and correspondingly C, C_s, C_v are expressed as

$$C = 0, 0, 4\text{sgn}(\lambda) \parallel C_s = 0, 0, 0 \parallel C_v = 0, -4\text{sgn}(U), 0, \quad (10)$$

where $\text{sgn}(x)$ is the sign function. For the SVP-QAH insulator, we calculate C_η^s to be

$$C_\eta^s = (\delta_{s,1} + \delta_{s,-1}) \left[\text{sgn}(\lambda)\delta_{s,\text{sgn}(U)} + s\eta\delta_{s,\text{sgn}(-U)} \right], \quad (11)$$

and the other Chern numbers satisfy

$$C = 2\text{sgn}(\lambda), \quad C_s = 2\text{sgn}(\lambda U), \quad C_v = -2\text{sgn}(U). \quad (12)$$

Here, $\delta_{\mu,\nu}$ is the Kronecker delta function. We see from Eqs. (9) and (11), $|C_\eta^s| = 1$ always holds for each TI case.

To distinguish and detect the SVP-QAH state, we consider a domain wall between AB- and BA-stacked GBL [15] in Fig. 3(a), where the conducting channels and band structure are shown when λ has the opposite values in AB and BA regions. By using Green's function method [37], we show the domain-wall conductance [$G = I/V$, where $I(V)$ is the current

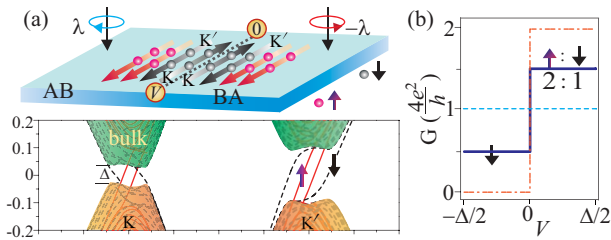


FIG. 3: (Color online) (a) Sketch of a domain wall (top) between AB- and BA-stacked BLG. The voltage $V(0)$ is for detection. The conducting channels are shown for the AB(λ)/BA($-\lambda$) case, where the band structure (bottom) is calculated for a sharp domain wall. The band gap satisfies $\Delta \approx \min \Delta_{\eta}^s(\eta, s = \pm 1)$. (b) Domain-wall conductance within the gap in the AB(λ)/BA($-\lambda$) domain walls. The solid, dashed, dot-dashed lines represent, respectively, the SVP-QAH, QAVH (the same for QVH) and N-QAH cases.

(bias)] in Fig. 3(b) and predict a unique spin rectification effect (solid line) for the SVP-QAH edge states. We assume here that the domain wall is much shorter than the electron mean free path, and thus scattering is ignored. The ratio of channel numbers for \uparrow and \downarrow is 2 : 1 for $V > 0$, while only \downarrow channels contribute to transport for $V < 0$. In contrast, no charge or spin rectifications (dashed line) occur for the QAVH or QVH states. The N-QAH state acts as a charge diode, however, still no spin rectification occurs. The spin or valley filter and spin diode can be further realized by modulating the domain-wall types and external fields (Supplemental Material [32]).

Note that all the QVH channels marked by K and K' in Figs. 2(a)-2(d) and 3(a) disappear along the armchair direction [9, 10, 12] when valley is not a good quantum number. Nevertheless, a unipolar spin diode [38] (only spin-up electrons are unidirectionally conducting for $V > 0$) works if the domain wall is of the armchair type in Fig. 3(a).

Discussion.—Realization of the SVP-QAH state in BLG depends on the presence of the magnetic field term, H_M , which is not induced by the electron-electron interaction [26] but by proximity, such as a van der Waals system consisting of BLG and magnetic insulator CrI_3 [30] ($M \sim 7$ meV can be achieved). Possibilities of proximity induced by other 2D layered magnets in BLG, such as CrBr_3 or $\text{Cr}_2\text{Ge}_2\text{Te}_6$ [39], requires more research. Magnetic insulator EuS is an alternative candidate to induce H_M on basis of the experimental evidence for ferromagnetism in graphene [40]. Beyond model (1), the Coulomb interaction might induce a gap about 1 meV [7, 26], which is usually disregarded when other interactions are stronger [4, 15–17] as we concern in Eq. (1).

In particular, other photoinduced terms beyond H_λ such as optical absorption and high-energy Floquet sidebands [34, 41, 42] can be safely ignored [25–27, 34] as we focus on the nearly off-resonant light above 10 THz. Because the light absorbance per graphene layer is only about 2.3% [43], the band population is presumably intact. For the SVP-QAH domain-wall transport in Fig. 3(a), the electron mean free path $L_0 \sim 420$ nm is verified by experiment [15–18]. Ignoring

the contact resistance, the dependence of ballistic conductance G on domain-wall length L is determined by [15, 37] $G = (\zeta e^2/h)(1 + L/L_0)$, where ζ corresponds to the integer for quantized plateau as given in Fig. 3(b).

The topological transitions modulated by photon and electric voltage explored here will motivate the experimental exploration of novel 2D QAH insulators with rich spin or valley physics based on BLG as well as the integrated systems between layered 2D materials, van der Waals magnets and correlated valley materials, for which the combination of spintronics, valleytronics and topology promises discoveries of novel condensed matter phases.

This work was supported by the NSFC with Grant No. 61874057, QingLan Project of Jiangsu Province (2019), 1311 Talent Program “DingXin Scholar” of NJUPT (2018), and Jiangsu Government Scholarship for Overseas Studies.

-
- [1] T. Ohta, A. Bostwick, T. Seyller, K. Horn, and E. Rotenberg, *Science* **313**, 951 (2006).
 - [2] K. S. Novoselov, E. McCann, S. V. Morozov *et al.*, *Nat. Phys.* **2**, 177 (2006).
 - [3] E. McCann, *Phys. Rev. B* **74**, 161403(R) (2006).
 - [4] Y. Zhang, T.-T. Tang, C. Girit *et al.*, *Nature* **459**, 820 (2009).
 - [5] I. Martin, Y. M. Blanter, and A. F. Morpurgo, *Phys. Rev. Lett.* **100**, 036804 (2008).
 - [6] R. T. Weitz, M. T. Allen, B. E. Feldman, J. Martin, and A. Yacoby, *Science* **330**, 812 (2010).
 - [7] J. Velasco Jr, L. Jing, W. Bao *et al.*, *Nat. Nanotechnol.* **7**, 156 (2012).
 - [8] E. McCann and M. Koshino, *Rep. Prog. Phys.* **76**, 056503 (2013).
 - [9] Y. Ren, Z. Qiao, and Q. Niu, *Rep. Prog. Phys.* **79**, 066501 (2016).
 - [10] L. Ju, and L. Wang, T. Cao *et al.*, *Science* **358**, 907 (2017).
 - [11] W. Jaskólski, M. Pelc, G. W. Bryant, L. Chico, and A. Ayuela, *2D Mater.* **5**, 025006 (2018).
 - [12] F. Zhang, A. H. MacDonald, and E. J. Mele, *Proc. Natl. Acad. Sci.* **110**, 10551 (2013).
 - [13] F. Zhang, J. Jung, G. A. Fiete, Q. Niu, and A. H. MacDonald, *Phys. Rev. Lett.* **106**, 156801 (2011).
 - [14] X. Li, F. Zhang, Q. Niu, and A. H. MacDonald, *Phys. Rev. Lett.* **113**, 116803 (2014).
 - [15] L. Ju, Z. Shi, N. Nair *et al.*, *Nature* **520**, 650 (2015).
 - [16] J. Li, K. Wang, K. J. McFaul *et al.*, *Nat. Nanotechnol.* **11**, 1060 (2016).
 - [17] L.-J. Yin, H. Jiang, J.-B. Qiao, and L. He, *Nat. Commun.* **7**, 11760 (2016).
 - [18] L. Jiang, Z. Shi, B. Zeng *et al.*, *Nat. Mater.* **15**, 840 (2016).
 - [19] Z. Qiao, W.-K. Tse, H. Jiang, Y. Yao, and Q. Niu, *Phys. Rev. Lett.* **107**, 256801 (2011).
 - [20] X. Zhai and G. Jin, *Phys. Rev. B* **93**, 205427 (2016).
 - [21] C.-Z. Chang, J. Zhang, X. Feng *et al.*, *Science* **340**, 167 (2013).
 - [22] M. Ezawa, *Phys. Rev. Lett.* **109**, 055502 (2012).
 - [23] X. Zhai and G. Jin, *Phys. Rev. B* **89**, 235416 (2014).
 - [24] W.-K. Tse, Z. Qiao, Y. Yao, A. H. MacDonald, and Q. Niu, *Phys. Rev. B* **83**, 155447 (2011).
 - [25] P. Mohan and S. Rao, *Phys. Rev. B* **98**, 165406 (2018).
 - [26] C. Qu, C. Zhang, and F. Zhang, *2D Mater.* **5**, 011005 (2018).

- [27] V. Dal Lago, E. S. Morell, and L. E. F. Foa Torres, Phys. Rev. B **96**, 235409 (2017).
- [28] H. Pan, Z. Li, C.-C. Liu, G. Zhu, Z. Qiao, and Y. Yao, Phys. Rev. Lett. **112**, 106802 (2014).
- [29] J. Zhou, Q. Sun, and P. Jena, Phys. Rev. Lett. **119**, 046403 (2017).
- [30] C. Cardoso, D. Soriano, N. A. García-Martínez, and J. Fernández-Rossier, Phys. Rev. Lett. **121**, 067701 (2018).
- [31] F. D. M. Haldane, Phys. Rev. Lett. **61**, 2015 (1988).
- [32] See Supplemental Material for details on inducing of H_{\pm} bands in a zigzag ribbon, and realization of spin or valley filter, spin diode by modulating the light-voltage and domain-wall types.
- [33] T. Kitagawa, T. Oka, A. Brataas, L. Fu, and E. Demler, Phys. Rev. B **84**, 235108 (2011).
- [34] M. Ezawa, Phys. Rev. Lett. **110**, 026603 (2013).
- [35] Y.-W. Son, M. L. Cohen, and S. G. Louie, Nature **444**, 347 (2006).
- [36] X. Zhai and G. Jin, Phys. Rev. B **89**, 085430 (2014).
- [37] S. Datta, *Electronic Transport in Mesoscopic Systems* (Cambridge University Press, Cambridge, England, 1995).
- [38] X. Zhai, R. Wen, X. Zhou, W. Chen, W. Yan, L.-Y. Gong, Y. Pu, and X. Li, Phys. Rev. Appl. **11**, 064047 (2019).
- [39] C. Gong and X. Zhang, Science **363**, 706 (2019).
- [40] P. Wei, S. Lee, F. Lemaitre *et al.*, Nat. Mater. **15**, 711 (2016).
- [41] M. A. Sentef, M. Claassen, A. F. Kemper *et al.*, Nat. Commun. **6**, 7047 (2015).
- [42] Y. H. Wang, H. Steinberg, P. Jarillo-Herrero, and N. Gedik, Science **342**, 453 (2013).
- [43] K. F. Mak, M. Y. Sfeir, Y. Wu, C. H. Lui, J. A. Misewich, and T. F. Heinz, Phys. Rev. Lett. **101**, 196405 (2008).